SCIENCE CHINA
Physics, Mechanics & Astronomy

•Invited Review•
Special Topic: Microscopic Mechanism for Manipulating Thermal Conduction

November 2022 Vol. 65 No. 11: 117002
https://doi.org/10.1007/s11433-022-1952-3

Emerging theory and phenomena in thermal conduction: A selective review

Jie Chen[1], Jia He[1], Dongkai Pan[2], Xiaotian Wang[3], Nuo Yang[2], Jiaojiao Zhu[4], Shengyuan A. Yang[4], and Gang Zhang[5*]

[1] *Center for Phononics and Thermal Energy Science, China-EU Joint Lab for Nanophononics, MOE Key Laboratory of Advanced Micro-structured Materials, School of Physics Science and Engineering, Tongji University, Shanghai 200092, China;*
[2] *School of Energy and Power Engineering, Huazhong University of Science and Technology (HUST), Wuhan 430074, China;*
[3] *School of Physical Science and Technology, Southwest University, Chongqing 400715, China;*
[4] *Research Laboratory for Quantum Materials, Singapore University of Technology and Design, Singapore 487372, Singapore;*
[5] *Institute of High Performance Computing, Agency for Science, Technology and Research (A*STAR), Singapore 138632, Singapore*

Received February 21, 2022; accepted July 4, 2022; published online October 8, 2022

Recently, emerging phonon phenomena have been discovered and rapidly developed, which have become an active hot research topic. In this review article, we present state-of-the-art advances in several fascinating phonon transport phenomena. First, we summarize the recent progress on the wave nature of phonons, including phonon coherence and its effects on thermal conductivity and the topological properties of phonons. Then, we discuss the particle nature of phonons, including the weak coupling of phonons and the high-order phonon anharmonicity. Finally, we present the summary and a brief outlook. This review presents the advanced understanding of some emerging phonon phenomena in solid materials, which provides new opportunities for further advancement in a wide variety of applications.

phonon transport, coherence, topological phonon, high-order phonon interaction

PACS number(s): 63.20.Kr, 63.20.Ls, 63.22.+m, 63.20.-e, 66.70.+f

Citation: J. Chen, J. He, D. Pan, X. Wang, N. Yang, J. Zhu, S. A. Yang, and G. Zhang, Emerging theory and phenomena in thermal conduction: A selective review, Sci. China-Phys. Mech. Astron. **65**, 117002 (2022), https://doi.org/10.1007/s11433-022-1952-3

1 Introduction

The continuous miniaturization and integration of devices result in an escalated power density in electronic devices, which makes the manipulation and control of heat transport an important research topic in modern technology and industrial applications [1]. Materials with high thermal conductivity can be used for heat dissipation in electronic devices [2], whereas thermoelectric materials pursue a low thermal conductivity [3,4]. Thermal transport has been described on the basis of Fourier's law. Interestingly, many novel thermal conduction phenomena in nanostructures that violate Fourier's law have been observed in the past decades and have attracted considerable attention [5-8]. For example, the anomalous heat conduction phenomenon is reported in silicon nanowires based on molecular dynamics simulation [9]. This anomalous heat conduction leads to the peculiar size-dependent thermal transport in low-dimensional materials [6].

In recent decades, experimental, theoretical, and computational developments have promoted the understanding of nanoscale heat conduction [10-30]. Recent advances in

*Corresponding author (email: zhangg@ihpc.a-star.edu.sg)

various interesting phonon phenomena, such as hydrodynamic phonon transport [31-33], coherent phonon transport [34-36], interfacial thermal transport [1], and phonon-magnon interaction [37], have been reviewed. Moreover, emerging phonon phenomena similar to electron transport have been discovered, such as hydrodynamic phonon transport [31,32], phonon coherence [26,38], weak coupling [39], and topological and high-order anharmonicity of phonon [40-45]. These novel phonon transport phenomena are active hot research topics and are developing rapidly, which have received considerable attention.

In this review, we present state-of-the-art advances in the following phonon transport phenomena. To begin with, we discuss the wave nature of phonons, which includes the phonon coherence in sect. 2 and topological properties of phonons in sect. 3. Then we move to the discussion on the particle nature of phonons in terms of phonon-phonon coupling. In sect. 4, we review the recent advances on the phonon weak coupling of phonons. Sect. 5 introduces the effect of higher-order phonon anharmonicity on thermal transport. Finally, we present in sect. 6 the summary and a brief outlook for future studies.

2 Phonon coherence

Thomas Young's double-slit optics experiment demonstrates the interference patterns caused by wave coherence. With the development of related theories and experiments, the effect of wave interference is observed in various forms from light to acoustics. Phonons, as thermal energy carriers, have the characteristics of particles and waves. The particle nature of phonons, namely, the incoherent scattering picture, can be well described by the Boltzmann transport equation combined with first-principle calculations when the system length is longer than the phonon coherence length [13,14,46-50], based on a large number of experimental results [40-42]. When the characteristic length is less than or comparable to the wavelength of the thermal phonon, the wave behavior of the thermal phonon will emerge. With the development of nanotechnology in recent years, the wave nature of phonons has been observed in experiments [23,51-54].

2.1 Phonon interference effects

Traditional methods for reducing thermal conductivity primarily focus on the enhancement of phonon scatterings via incoherent mechanisms [11,55-60]. However, this approach might also deteriorate the electrical performance of the electronic device. The manipulation of phonon transport using the coherent mechanism is a potential approach for thermoelectric applications because it can suppress phonon thermal conductivity while keeping the electronic counterpart. Therefore, the wave-related phonon physics on the manipulation of heat transport receives considerable attention because of its great application potential [61-66].

To date, various coherent heat conduction phenomena in nanomaterials have been reported [17,67-70]. The coherent phonon transport is observed indirectly by the characterization of macroscopic variables, such as the non-monotonic variation of the thermal conductivity with the period length in phononic crystal structures [36,52], the variation of thermal conductivity with boundary roughness [71] or aperiodic structures [54,72], and temperature oscillation effect in superlattice [73]. Interested readers can refer to recent reviews [34-36] on the effect of coherent phonon transport on thermal conductivity. Moreover, phonon coherence manifests in various ways, such as hybridized phonon modes, phonon localization, and modal phonon interference. In this work, we will review the recent advances on phonon coherence in richer behaviors in addition to the variation of thermal conductivity, which will strengthen our understanding and utilization of coherent heat transport.

The introduction of guest atoms to cage materials can increase the thermoelectric performance of the host-guest system (HGS), which results from the reduction of the lattice thermal conductivity by the interaction between host cages and guest atoms. Based on the density functional theory and molecular dynamics simulations, Zhang et al. [74] unveiled the underlying physical mechanism for regulating thermal transport in HGS. As shown in Figure 1(a), the distinct hybridization modes (flat band in the shadowed region) appear in phonon dispersion, whereas the phonon density of states further reveals that the hybridization mode is contributed by the motion of the guest atom. This mode hybridization remarkably reduces the phonon group velocity (non-propagating flat band) and is responsible for the decrease in thermal conductivity.

In addition, Davis et al. [75] demonstrated that hybridized resonance phonon modes could be found in silicon thin film with a nano-pillar structure. Figure 1(b) shows the phonon dispersion of silicon thin film with pillars, in which the nanoscale pillars serve as local resonant units interacting with the thin film. Consequently, the resonance between the heat phonon waves in the thin film and the local phonon modes in the pillars leads to several hybridization modes appearing in the low-frequency region of the phonon dispersion (Figure 1(b)). Similar to the HGS, the frequency of hybridized modes can be adjusted by changing the shape and size of the pillar. Moreover, Ma et al. [76] found that the isotopic resonance in pillars can induce a mismatch between the resonant modes and propagating modes, which leads to the breaking of phonon mode hybridization. Thereafter, hybridization modes by resonant thermal phonon in pillar-based metamaterial have been extensively explored [77-80]. Those studies indicate that the hybridization modes not only

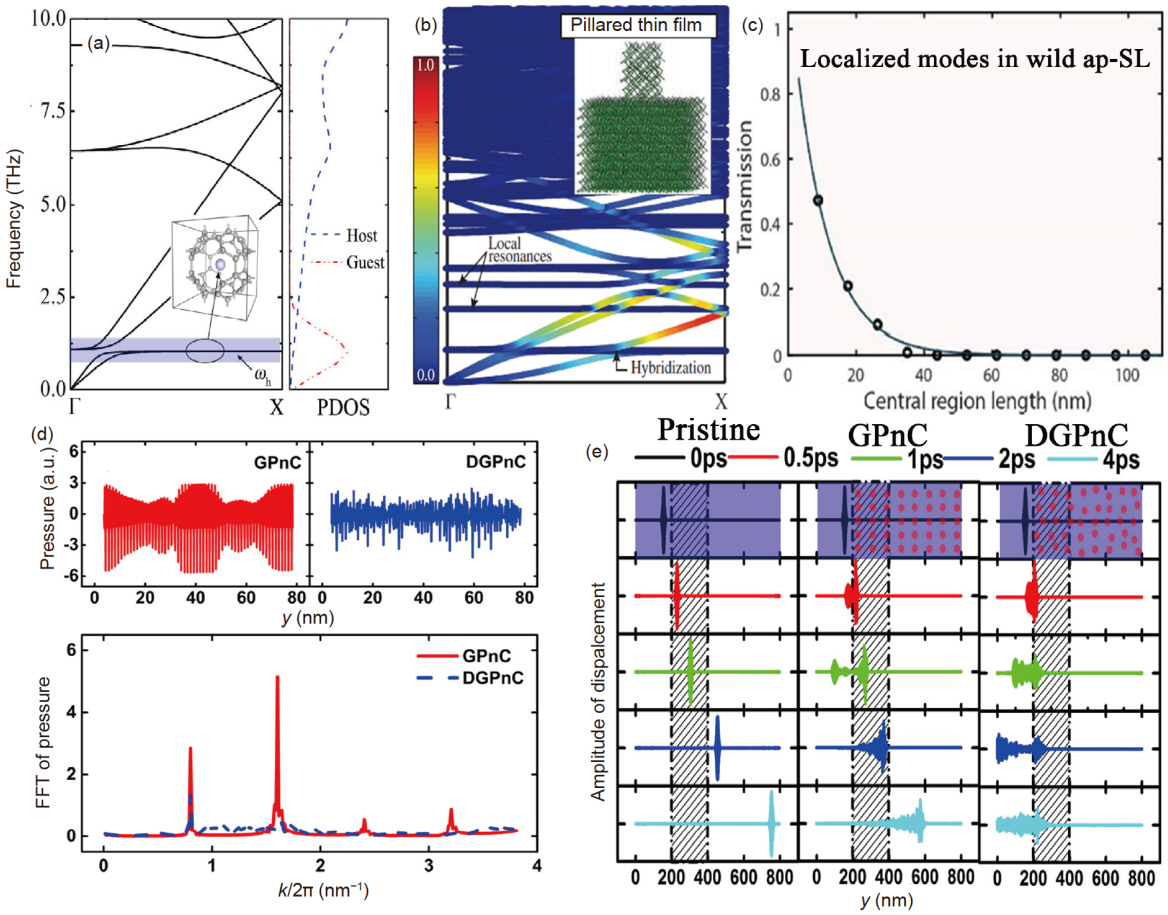

Figure 1 (Color online) (a) Phonon dispersion and phonon density of states for the host-guest system. The inset shows the atomic structure of the host-guest system [74]. (b) Phonon dispersion of pillared silicon nano-phononic crystals. The inset shows the atomic structure of the pillared thin film. Here different colors represent the modal contribution to the cumulative thermal conductivity [75]. (c) Phonon transmission as a function of system length for localized modes [86]. (d) Spatial distribution of pressure in GPnC (graphene phononic crystals) and DGPnC (disordered graphene phononic crystals) at 300 K [87]. (e) Phonon wave packet simulations in pristine graphene, namely, GPnC and DGPnC. The dashed line at y = 200 nm denotes the interface, and the red dots indicate the holes [87].

affect the phonon group velocity but also decrease the phonon lifetime around the frequency of hybridization modes.

Anderson [81] discussed the motion of electrons in disordered crystals in 1958 and proposed the concept of electron localization in disordered atomic systems. As the thermal energy carrier, phonon and its localization have attracted research interest. Based on the wave behavior of phonon, phonon localization has been widely studied in the field of thermoelectric materials because phonon localization provides a new approach to obtain materials with low thermal conductivity [82-85]. For example, Hu et al. [86] studied the scaling of phonon Anderson localization based on the system length in Si/Ge aperiodic superlattices. Using atomistic Green's function, they obtained the transmission coefficient of ballistic modes, propagating modes, and localized modes. The transmission coefficient of the ballistic mode has no relationship with the system length, and the propagating modes are less dependent on length. For localized modes, the phonon transmission coefficient decays exponentially with the increase of system length (Figure 1(c)), indicating phonon localization.

In addition to the scaling behavior, Hu et al. [87] demonstrated that phonon localization can be directly captured through spatial distribution of pressure and phonon wave packet simulation in disordered graphene phononic crystal (DGPnC) and graphene phononic crystal (GPnC). As shown in Figure 1(d), they found that the spatial distribution of pressure in GPnC is periodically modulated along the transport direction, and this behavior is present at different time snapshots. By performing the Fourier transform of the spatial distribution, they further revealed that the periodic modulation in the coordinate space originates from the discrete peaks found in the reciprocal space, and the wavelength λ of the peak is related to the period length L_0 as $\lambda=L_0/n$ (n is an integer), indicating the coherent phononic behavior in GPnC. By contrast, no evident spatial pressure modulation is observed in DGPnC, and only one notable peak remains in reciprocal space. This remaining peak results from the pho-

non localization induced by the disorder. They further launched the phonon wave packet of this particular mode and monitored its propagation to verify this point. As shown in Figure 1(e), the launched phononic wave packet travels at constant velocity and keeps its shape unchanged in pristine graphene. For graphene/GPnC, the wave packet is splitted into the reflected wave and transmitted wave at the interface (y = 200 nm), whereas the transmitted wave can still propagate across GPnC. When the same wave packet passes through the interface between graphene and DGPnC, the wave packet is trapped near the interface region, and it cannot propagate forward, indicating the localized behavior of this particular phonon mode. Furthermore, Juntunen et al. [88] found that the localization of phonons can be manifested as the formation of dense mini-band at Brillouin zone edges.

Recently, Guo et al. [89] found a partial localization phenomenon in graded superlattices. Compared with full phonon localization, partial localization decays the phonon transmission coefficient to a non-zero value with the increase of superlattice length. The short-range order and long-range disorder in graded superlattices result in the strong anharmonicity of high-frequency phonons, which destroy phonon coherence; thus, no complete localization is achieved. Furthermore, the degree of disorder may be a key factor in controlling phonon localization.

A quantitative understanding of phonon hybridization and localization is important to control the thermal transport properties. In the HGS model, Zhang et al. [74] reported that the eigenfrequency of the hybridization mode is calculated as $\omega_{\mathrm{h}} = \sqrt{\frac{K_{\mathrm{e}}}{m}\left(1+\frac{m}{M}\right)}$, where K_{e} is the effective force constant between the host cage and guest atom, and m and M are the mass of the guest atom and host cage, respectively. When the mass of the host cage is larger than that of the guest atom (M>>m), this eigenfrequency can be simplified as $\omega_{\mathrm{h}} \approx \sqrt{K_{\mathrm{e}}/m}$. Therefore, the frequency of the hybridization mode is determined by the coupling strength and mass of the guest atoms. By varying these two physical parameters, hybridization modes at specific frequencies can be obtained. As shown in Figure 2(a), when matching the hybridization mode frequency with the phonon frequency that dominates the thermal transport in the host system (ω_1 and ω_2), the maximum reduction of thermal conductivity in HGS can be achieved with the introduction of a single hybridization mode. Furthermore, multiple hybridization modes at different frequencies can be introduced simultaneously to suppress multiple dominant peaks in spectral thermal conductivity (Figure 2(b)), providing a general guideline to reduce the thermal conductivity of realistic materials via the hy-

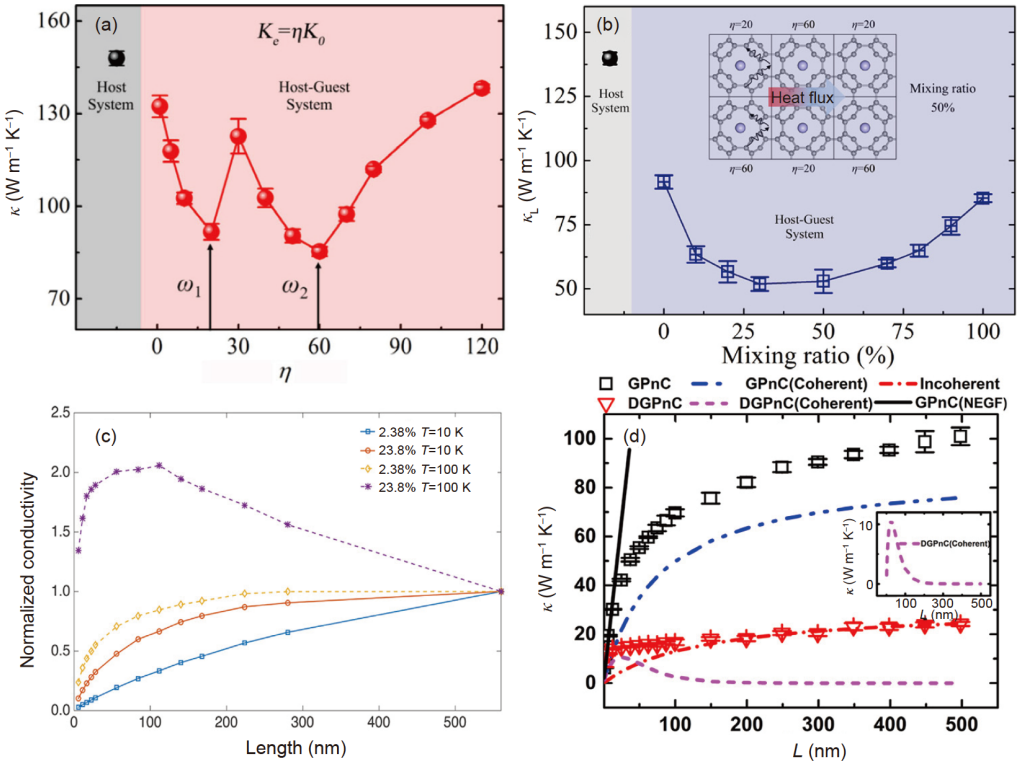

Figure 2 (Color online) (a) Tunable lattice thermal conductivity with a single hybridization mode by varying the coupling constant defined by $K_{\mathrm{e}} = \eta K_0$ [74]. (b) Reduced lattice thermal conductivity with two hybridization modes with frequency ω_1 and ω_2. The inset illustrates the host-guest system with a mixing ratio of 50% [74]. (c) Normalized thermal conductivity versus the length of GaAs/AlAs superlattice. Here the ErAs interfacial coverage is 2.38% and 23.8%, respectively, at 10 and 100 K. Anderson localization results in the local thermal conductivity maximum [84]. (d) Decomposed coherent and incoherent contribution to the thermal conductivity of GPnC and DGPnC. The inset shows the coherent contribution [87].

bridization mode.

Phonon Anderson localization can provide a minimized thermal conductivity lower than the theoretical minimum in the particle-like picture [90]. As shown in Figure 2(c), at low temperatures and low degrees of disorder, the thermal conductivity of disordered superlattices increases monotonically with increasing system length because long-wavelength phonon dominates heat conduction. On the contrary, in highly disordered superlattices at high temperatures, the localized modes become populated, and the exponential decaying nature of the localized modes decreases the thermal conductivity with the system length. These two competing mechanisms lead to the maximized thermal conductivity with regard to the total length observed in superlattices with a high degree of disorder at high temperatures [84,85]. Moreover, for partial phonon localization in graded superlattices [89], the thermal conductivity decreases with length at the initial stage because the strongly elastic backscattering is faster than the quantum diffusion limit. Then, the thermal conductivity increases with an increasing number of the period because the convergence of thermal conductance is stronger than the partial phonon localization. The competition mechanism between localization and ballistic heat conduction leads to a local minimum of the thermal conductivity in the graded superlattice.

In phononic crystal structures, the individual interface/hole serves as the scattering center based on the incoherent mechanism, whereas the periodic arrangement of the interface/hole allows for coherent phonon manipulation. Therefore, incoherent and coherent phonon transport can coexist in such a periodic structure. In quantitatively evaluating the incoherent and coherent phonon contribution, Wang et al. [91] proposed a two-phonon model, which divides all phonons into two groups (coherent and incoherent) using the following equation:

$$\begin{aligned}\kappa(L) &= \kappa_{\mathrm{coh}}(L) + \kappa_{\mathrm{inc}}(L) \\ &= LG_{\mathrm{coh},0}\frac{l_{\mathrm{coh}}}{l_{\mathrm{coh}}+L} + LG_{\mathrm{inc},0}\frac{l_{\mathrm{inc}}}{l_{\mathrm{inc}}+L},\end{aligned} \tag{1}$$

where G_0 denotes the ballistic limit thermal conductance; L is the system length, and l_{coh} and l_{inc} are the mean free path of coherent and incoherent phonons, respectively. The microscopic definition of phonon coherence length can be found in the work by Latour et al. [92]. When introducing a disorder to the system, the coherent phonon will be localized because of the wave nature. Phonon localization results in the exponential decay of the coherent contribution with the increase of system length, which is calculated as $LG_{\mathrm{coh},0}\frac{l_{\mathrm{coh}}}{l_{\mathrm{coh}}+L}\mathrm{e}^{-L/l_{\mathrm{loc}}}$, where l_{loc} is the phonon localization length. Therefore, the coherent contribution will vanish when the system length is longer than the phonon localization length. By comparing the thermal conductivity values without and with the disorder in the large L limit, the contribution of coherent and incoherent phonon can be obtained.

Based on the two-phonon model, Hu et al. [87] found that coherent phonon transport dominated the heat conduction in the GPnC structure at 300 K. As shown in Figure 2(d), the contribution of the coherent phonon is more than 80% of the thermal conductivity of the GPnC structure at room temperature [87]. In contrast to the conventional picture, showing that the critical period (corresponding to the minimum thermal conductivity) separates the coherent and incoherent transport region in the superlattice structure, their simulation results reveal that the coherent contribution can penetrate into the incoherent region, which is only negligible when the superlattice period length is longer than the critical period [87]. These results highlight the importance of coherent phonon transport in periodic structures.

The wave behavior of coherent phonons is not only indirectly reflected via macroscopic thermal transport properties but also manifested at microscopic mode-level interference. Jiang et al. [93] systematically studied the interference effect of individual phonons in graphene superlattice with isotopic carbon atoms. Their wave packet simulations demonstrated the constructive and destructive mode-level interference among the reflected phonons, leading to the valleys and peaks in the phonon transmission coefficient, respectively. As shown in Figure 3(a), the total transmission and total reflection of individual phonons can be achieved. Similar to the interference effect of the optical and acoustic waves, the superlattice period L_{p} and phonon wavevector q_x^s must satisfy the following interference condition:

$$\frac{L_{\mathrm{p}}\times q_x^s}{2\pi} = \frac{m}{4}, \tag{2}$$

where m is an integer corresponding to the valleys and peaks in phonon transmission. Moreover, maintaining phononic monochromaticity and multiple scatterings are necessary to enhance the phonon interference effect.

In addition to the superlattice structure, Hu et al. [94] proposed an approach based on two-path phonon interference to achieve a stop band and the total reflection of the phonons in a multilayer array with a crystalline silicon matrix and embedded germanium nanoparticles. As shown in Figure 3(b), the phonon transmission decreases dramatically as the number of nanoparticle layers increases. Considering ten nanoparticle layers, a stop band prohibiting the phonon transmission eventually arises at 1.9 THz. Using wave packet simulations, they further confirmed that the phonon wave packet with a frequency of 1.9 THz is nearly totally reflected by the nanoparticle multilayer array because of the collective phonon resonance. Moreover, the space among adjacent germanium nanoparticles must be equal to the half wavelength of the phonon in the crystalline silicon matrix.

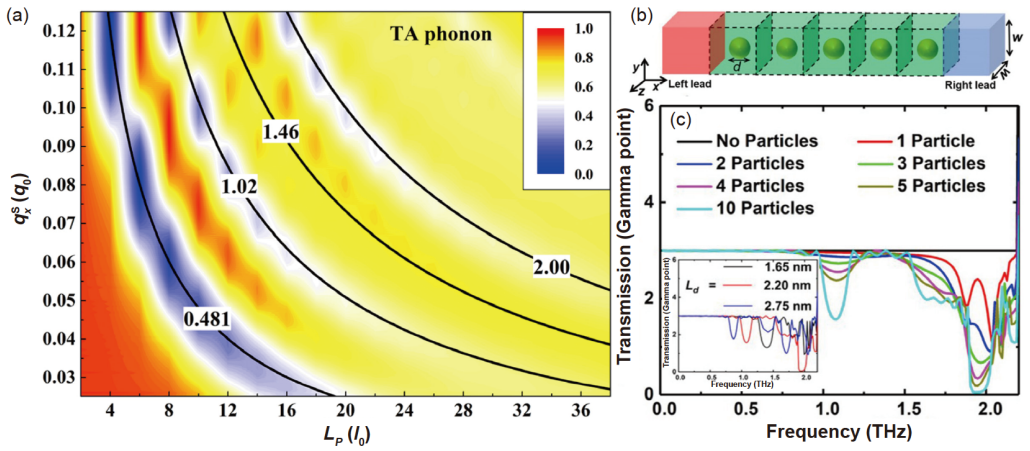

Figure 3 (Color online) (a) Color contour plot of the transmission function for the transverse acoustic phonon with different superlattice wavevectors and period lengths. Black solid lines show the hyperbolic fitting [93]. (b) A schematic picture of the quasi-1D silicon crystal matrix with embedded nanoparticles. (c) Low-frequency phonon transmission function for two-path interference phononic crystals. (b) and (c) from ref. [94].

Compared with the classic superlattice structure, phonon coherence can be achieved in the two-path phonon interference without strict requirements on periodicity. Therefore, the two-path phonon interference provides a novel avenue to understand the coherent phonon transport. These studies on mode-level interference provide valuable insights into the design of phononic functional devices [95-99] based on the wave behavior of phonons.

2.2 Inter-band phonon correlation

The mode-level correlation behavior of thermal phonons is also observed in complex crystals [38,100-104] because of the inter-band off-diagonal contribution. Notably, the physical origin of "phonon coherence" in superlattice is different, which is due to the wave interference effect. Following the term used in many references, in this section, we defined the mode-level correlation behavior as coherence. Such phonon coherence also has a significant effect on thermal conductivity. Simoncelli et al. [100] derived a general theory for thermal conduction in complex crystals from the Wigner distribution of quantum mechanics. The complex crystals do not have a well-separated phonon branch. Therefore, the inter-band interval is less than the phonon linewidth. In this work by Simoncelli et al. [100], the intra-band phonon and inter-band phonon were defined as populations and coherences, respectively. The intra-band contribution to thermal conductivity is dominated by the particle-like behavior of phonons, whereas the inter-band contribution is dominated by the wave-like coherent behavior. As shown in Figure 4(a), they calculated the thermal conductivity of the complex crystal $CsPbBr_3$ as a function of temperature by this general theory combined with first-principle calculations. Interestingly, the contribution of the coherence part increases with the increase in temperature. The population part contributes 30% of the total thermal conductivity, whereas the coherence part contributes 70% at room temperature. The total thermal conductivity of $CsPbBr_3$ calculated by their theory is consistent with the experimental values because of the accurate modeling of the coherence part. Moreover, the mode-level analysis found that the contribution of populations is primarily from low-frequency phonons with strong dispersion, whereas all of the phonon branches contribute to the coherence part. In addition, Isaeva et al. [101] developed a similar approach by molecular dynamics, and they have reached a similar conclusion. Later, Jain [102] calculated the thermal conductivity of the complex crystal Tl_3VSe_4 based on the recently proposed multichannel thermal conduction model. After considering the contribution of the coherent phonon transport channels, the predicted thermal conductivity is consistent with the experimental result. The contribution of wave-like heat conduction is two times that of the particle-like phonon transport.

Recently, Zhang et al. [38] proposed a general heat conduction theory that includes two types of phonon coherence by equilibrium molecular dynamics simulation and wavelet transformation of atomic trajectories. This theory is based on the generalized phonon decay law [103], which provides new insight into the phonon coherence in complex crystals, such as Tl_3VSe_4. In general, the intrinsic coherent behavior of the phonons decreases with the increase of temperature, thereby reducing the coherence time. This result is consistent with the phonon coherence of the low-frequency modes (0.25 THz). However, for the high-frequency mode (0.93 THz) with high density (Figure 4(b)), coherence time is directly proportional to temperature (Figure 4(c)). By performing an analysis of the phonon lifetime and coherence time, they found that the expansion of the phonon linewidth and reduction of the phonon branch intervals promote smaller wave packets. Later, the odds of these wave packets

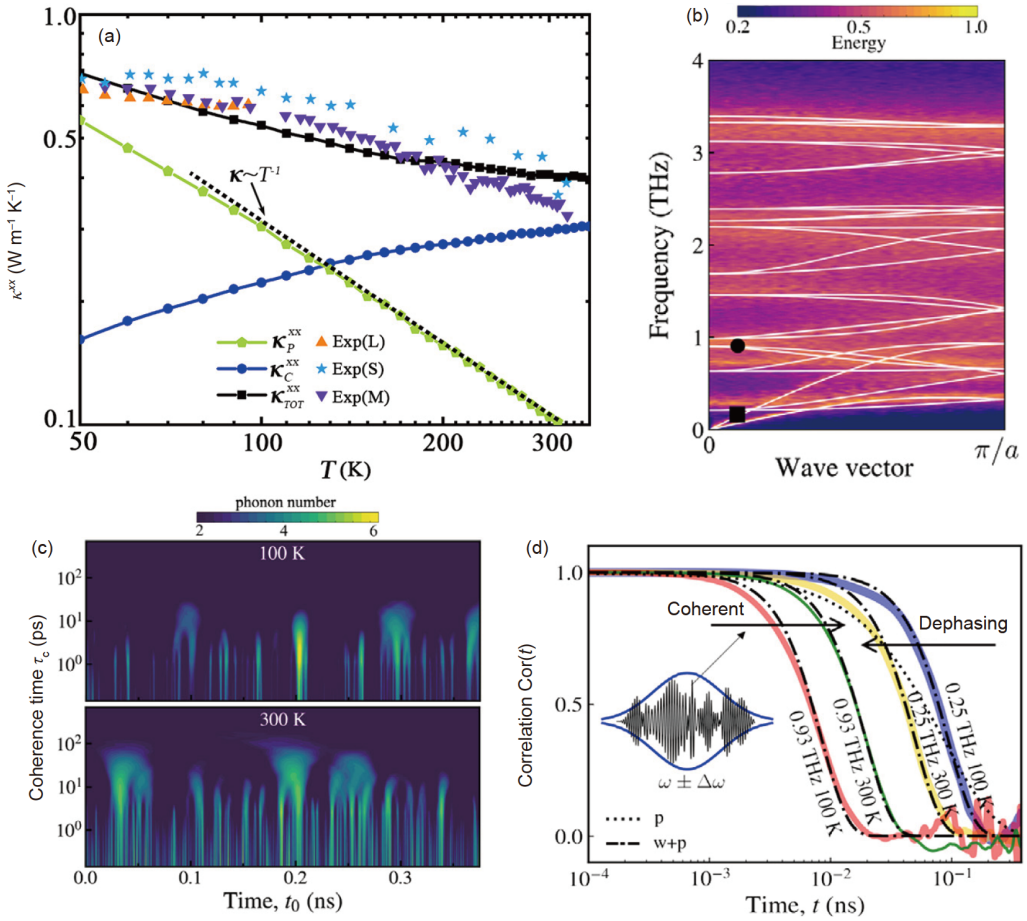

Figure 4 (Color online) (a) Temperature-dependent thermal conductivity of $CsPbBr_3$. Green: Peierls's LBTE conductivity; blue: thermal conductivity contributed by coherent phonons; black: total thermal conductivity. Adapted from ref. [100]. (b) Phonon dispersion of Tl_3VSe_4, with white lines indicating the lattice dynamic calculation results and contour indicating the spectral energy density calculation results. (c) Evolution-time and coherence-time-dependent phonon number for the 0.93 THz phonon mode in Tl_3VSe_4. (d) Phonon decay as a function of correlation time. The inset shows the realistic wave packet of the mode 0.93 THz resulting from the combination of shorter wave packets at 300 K. (b)-(d) from ref. [38].

establishing coherent relations with themselves become greater because of an increase in the number of wave packets, leading to a longer coherence time. This mutual phonon coherence is consistent with Simoncelli et al.'s [100] coherence model. In addition, for high-frequency mode with high phonon branch density, increased coherence with increasing temperature suppresses the decay of phonon transmission (Figure 4(d)).

Finally, the manipulation of coherent phonons can also be used to design phononic devices [95-99]. For example, Zhang et al. [95] reported a phonon nanocapacitor model for storing coherent phonons based on the phonon confinement effect of the hybridized mode in HGS, whereas the stored phonons can be emitted with the application of strain. In addition, the HGS can be utilized to build the phononic rectifier, in which asymmetric phonon transport can be achieved in different heat flow directions [96]. Furthermore, the coherent phonon state can be generated by the self-synchronization phenomenon via thermal noise [105] or by pulsed laser in the optomechanical system [106,107].

3 Topological phonons

Topology is a branch of mathematics studying properties that are preserved under the continuous deformation of objects. In solid materials, topology is flourished first in the sector of electrons. In the 1980s, the studies on the quantum Hall effect, particularly the work by Thouless et al. [108], revealed the topological character of the effect and highlighted the important geometric quantity, Berry curvature, and topological Chern invariant in the picture. Berry curvature is an intrinsic geometric quantity of electronic bands, which measures the eigenstate "curve" in the momentum space. For completely filled bands, for example, those below a band gap, its integral over the 2D Brillouin zone gives the Chern number, which is an integer characterizing the nontrivial "twist" of the wave functions and dictating the number of chiral edge channels. This characterization applies to 2D systems without any symmetry (except for the lattice translations that define the crystal). For example, symmetries (time reversal, particle hole, crystalline symmetries, etc.)

would constrain the wave functions in different ways and lead to different kinds of topological states [109-111], which have been the subject of extensive research in the past decades.

Phonon states are also described by Bloch wave functions, forming phonon band structures in the Brillouin zone. According to Zhang et al. [45], the Berry curvature can be similarly defined for phonons, which has been utilized to explain the phonon Hall effect [112]. Topological phonon states with nontrivial Chern numbers, analogous to the quantum Hall state, were also proposed [113].

It is worth mentioning that chiral phonon study related to symmetry and topology has an active branch in the past few years, i.e., those phonon modes having a sense of handedness. The concept was first proposed by Zhang and Niu [114] in a 2D honeycomb lattice model, which was generalized to other systems and materials [115-118]. These chiral phonons can selectively couple with valley electrons and circularly polarized photons [114]. Their effects have been confirmed in several optical experiments on 2D transition metal dichalcogenides materials [119-122]. Recently, propagating chiral phonon modes were reported in some intra-layer heterojunctions [123] and in 3D crystalline materials [124]. In particular, Chen et al. [125] proposed a chiral phonon diode effect, for which chiral materials such as bulk Te or α-quartz can serve as a diode for chiral phonon propagation. This finding leads to new possibilities for building quantum devices based on chiral phonons.

Meanwhile, extensive effort has been made to achieve topological states in artificial periodic systems such as acoustic crystals or mechanical networks [126-128], which are similar to the classical counterparts of phonons in solids. This field of research benefits from the advantages of artificial systems, which are easy to design, fabricate, and detect.

The large-scale generalization of topological notions to phonons in solids occurred relatively later. Phonon states analogous to 2D topological insulators were investigated in a model study, and efficient phonon transport through topological boundary channels was demonstrated [129,130]. Recently, Zhu et al. [131] predicted high-order topological insulator states (including real Chern insulator states) for phonons in graphene-based materials, where a finite-size sample has protected phonon modes localized at corners. More studies were on states analogous to topological semimetals, which feature protected degeneracies in the band structure. Based on the dimensionality of the phonon band crossing, the topological phonons can be divided into nodal point, nodal line, and nodal surface phonons with zero-, one-, and two-dimensional phonon band-crossings, respectively. Some representative material examples are listed in Table 1.

Weyl points always appear in pairs with opposite chirality. Wang et al. [132] proposed a topological triangular Weyl complex composed of one double Weyl point and two single Weyl points in the phonon dispersion of α-SiO_2. Charge-four Weyl point phonons characterized by Chern number ±4 are reported by Liu et al. [133] in realistic materials with space group numbers 195-199 and 207-214. Apart from two-, three-, and fourfold degenerate phonons, sixfold degenerate nodal point phonons are reported by Xie et al. [134]. A group of materials, including C_3N_4, Sc_4C_3, Y_4Sb_3, and K_8Si_{46}, are proposed to host the sixfold degenerate nodal point phonons. Chen et al. [135] systematically investigated three-dimensional Dirac phonons in all space groups with inversion symmetry. Some realistic materials are also proposed as potential materials with Dirac point phonons. Their work [135] provides a comprehensive understanding of three-dimensional Dirac phonons and essential guidance for exploring Dirac phonons.

Nodal line states in electronic systems are classified in accordance with the order of dispersion around a band degeneracy (linear, quadratic, and cubic) [136,137] and the slopes of crossing bands [138,139]. Similar to the electronic system, topological nodal line phonons can also be classified on the basis of the aforementioned perspectives. Recently, AgZr alloy [140] has been proposed to be a candidate material with hybrid-type nodal ring phonons and high-order quadratic nodal line phonons. Laves phase AB_2 with a C_{14} structure is proposed to host ideal type-III nodal ring phonons [141]. Moreover, based on symmetry arguments, a new type of hourglass phonons, jointly protected by symmorphic and nonsymmorphic symmetries, is demonstrated in $SrPt_3P$ [142]. Hourglass dispersion is usually under the projection of conventional nonsymmorphic symmetry. The reported hourglass state improved the understanding of topological phonons. Furthermore, some nodal structures, composed of more than one nodal line, are proposed in phonon states.

Table 1 Some predicted materials with nodal point, nodal line, and nodal surface phonons

Type of topological phonons	Some selected material candidates
Materials with higher-order topological insulator states for phonons	graphyne family materials [131]
Materials with nodal point phonons	SnO_2 [150], C_3N_4 [134], Sc_4C_3 [134], Y_4Sb_3 [134], K_8Si_{46} [134], SiO_2 [132], BiIrSe [133], Li_3CuS_2 [133], transition-metal monosilicides [44,144]
Materials with nodal line phonons	$SrPt_3P$ [142], MoB_2 [43], K_2O [156], ZnSb [148], RuS_2 [148], P_2Pt [148], OsS_2 [148], CuCl [143], FeS_2 [143], ZrAg [140], Li_6WN_4 [149], SnO_2 [150]
Materials with nodal surface phonons	SnO_2 [150], RbTeAu-family materials [146], $YCuS_2$ [145], $NiAs_2$ [145], $SrZrO_3$ [145], $LiAlO_2$ [145], ZnP_2 [145], NiSbSe [145], As_2Pt [145], $BaSi_2$ [145], $CsBe_2F_5$ [145]

Topological phononic nodal hexahedron net and nodal links are also found by Liu et al. [143] in CuCl. Experimentally, the double Weyl points in FeSi and nodal lines in MoB_2 were detected by inelastic X-ray scattering [43,144], which provided a strong driving force for this field.

In addition to materials with nodal point and nodal line phonons, one-, two-, and three-nodal surface phonons [145,146] are proposed in realistic materials, and practical routes for achieving one-, two-, and three-nodal surfaces in phonon systems are also given. Notably, the three-nodal surface phonons are good platforms for achieving a singular Weyl point phonon by circumventing the no-go theorem, as first proposed in ref. [147].

Moreover, some real-world materials are proven to host two or three types of degenerate dimensions in their phonon dispersion. It was [148] found that ZnSb (with space group number 61), RuS_2, P_2Pt, and OsS_2 (with space group number 205) exhibit Dirac nodal line net phonons and three-nodal surface phonons. Ref. [149] reported that the Li_6WN_4 feature nonsymmorphic symmetry projected a lantern-shaped nodal structure formed by the nearly flat nodal surface and nodal line structures in its phonon spectra. Using SnO_2 as an example and based on the first-principle calculations, Wang et al. [150] found that zero-, one-, and two-dimensional degeneracy phonon states can coexist in practical materials. Notably, the development of theoretical calculation methods also facilitates the screening of new topological phonon states. For example, a recent work by Li et al. [151] performed high-throughput calculations over 10000 materials, targeting degeneracies in the phonon bands.

Phonons are spinless bosons, following the bosonic statistics. This finding is contrary to electrons that are governed by the Fermi-Dirac distribution. In electronic systems, the topological features, such as nontrivial band gap or band degeneracies, must be close to the Fermi level to be detectable or manifested in physical properties because the involved energy scale is usually less than the Fermi energy. For phonons, no notion of Fermi level is observed, and the energy scale (< a few tens of meV) is smaller. This could be an advantage because the whole spectrum is experimentally accessible, and we are allowed to study topological band gaps or degeneracies anywhere in the spectrum. On the other side, this point could also be a disadvantage because isolating the contribution from the topological features in physical effects is difficult. For example, in the electronic case, a 2D topological insulator can have quantized conductance because the transport is restricted through topological edge channels. However, in the phonon case, the whole spectrum is usually involved in the phonon transport because of the absence of Pauli blocking. Then, separating the signal from the topological mode in the measured effect is difficult.

Therefore, future research must explore the unique physical properties of the topological phonon states. To date, the experiments on topological phonons were using inelastic X-ray scattering to image the topological band degeneracy [43,144]. Other measurable effects must be identified from the topological phonons to propose good material systems. Experimentally, new techniques must be developed to detect such effects. In particular, we need methods to single out the signal from topological modes.

The recently reported topological states for phonons were direct extensions from electronic systems. Phonons share the same topological classification as electrons in the absence of spin-orbit coupling, which has been systematically studied in the electronic context [109,152-154]. For example, using a group theory approach, Yu et al. [155] classified potential band degeneracy for the 230 space groups, which could be used to search or design a particular topological phonon mode. Meanwhile, finding topological states that exhibit the characteristics of phonons, which are distinct from electrons, is important. The recent work by Zhu et al. [156] provided an example in this direction. It shows that certain nodal chain degeneracies are enforced to exist in the phonon spectrum for a list of space groups by the vector basis characteristic of phonons, and their detection could benefit from the unique LO-TO splitting effect in ionic materials [156]. Such symmetry-enforced topological phonons could be an interesting direction to explore in subsequent research.

Finally, another future direction is the utilization of topological phonons for phononic devices. Some concepts have been explored in artificial systems, but the demonstration in real materials remains lacking. Therefore, the topological boundary mode must be utilized, either the 2D surface modes, 1D chiral modes, or 0D localized corner modes, for manipulating phonons.

4 Weak coupling

In sects. 2 and 3, we discuss the wave nature of phonons. Next, we move to the discussion on the particle nature of phonons with regard to phonon-phonon coupling, with sect. 4 focusing on the recent advances in weak coupling and sect. 5 focusing on high-order phonon coupling. Weak phonon coupling is an important mechanism that underlies many new phenomena in the heat conduction of low-dimensional/nanoscale systems [12,39,157-160]. The effect of weak coupling on phonon transport is manifested in several ways: on the one hand, weak phonon coupling reduces the scattering strength of phonons in the system, thereby enhancing the intrinsic thermal conductivity [39,157]. On the other hand, weak phonon coupling is an important factor that hinders the thermal conduction at van der Waals cross interfaces [161,162].

Here, the study of weak phonon couplings aims to bring a series of related new phenomena into a unified theoretical

understanding and framework. It will provide a novel perspective for the analysis of these phenomena. For a long time, certain phenomena, such as the size effect of thermal conductivity, the phonon non-equilibrium, and high thermal resistance in van der Waals cross interfaces, have been analyzed from distinct aspects and regarded as having no relationship. Therefore, they can hardly be studied under a unified framework. After systematic investigations, the phonon-phonon interactions in these phenomena are found to be remarkably weaker than those in traditional bulk systems. Therefore, weak phonon coupling is proposed. Moreover, it is an underlying physical mechanism behind a series of phenomena. By studying weak phonon couplings, various situations can be analyzed from a common perspective of physical mechanisms, breaking down the barrier between each other. Thus, breaking down the barrier among those new phenomena could predict more new phenomena in the future.

Weak phonon coupling within a single nanostructure has a strong correlation with the size effect of thermal conductivity, which indicates that the thermal conductivity of low-dimensional nanostructures is subject to the characteristic size of the system. The divergent size effect of thermal conductivity was first observed in the study of low-dimensional atomic chain models [8,163-168]. Later on, further studies of quasi-1D nanostructures such as nanowires and nanotubes [9,169-171] and two-dimensional materials [7,8,166] have shown that the size effect widely exists in low-dimensional systems. As the phonon scattering must be in accordance with the energy and quasi-momentum conservation, the scattering in nanomaterials is significantly suppressed. Therefore, the phonons tend to have a longer mean free path, making them more susceptible to the size of the system. Such size effects are contrary to the classical Fourier's law, in which thermal conductivity is treated as an intensive property independent of the system size [172]. In addition, weak phonon coupling can lead to different "temperatures" among different branches of phonons, namely, the multi-temperature phenomenon of phonons [173,174]. Models based on weak phonon coupling can provide an effective explanation for the phenomenon [157]. Meanwhile, the reduction of scattering rate caused by the weak coupling among different phonon branches in the system leads to a significant increase in the intrinsic thermal conductivity, which contributes to the enhancement of thermal transport. In recent years, graded thermal conductivity has been found in nanoscale graphene disks and carbon nanocones [175,176]. In the study of graded thermal conductivity, the graded thermal conductivity phenomenon tends to disappear when the coupling among phonons is enhanced, indicating that it is closely related to weak phonon coupling [177].

In addition, weak phonon coupling occurs between two or more nanostructures, such as van der Waals cross interfaces [178,179] and double-wall nanotubes [180,181]. The interaction at these interfaces is primarily due to the van der Waals force, which is weaker than the interatomic chemical bonds within the systems. Models based on weak phonon coupling can provide an effective explanation for the heat conduction at such interfaces [39,182,183], which emphasizes the importance of weak phonon coupling in the thermal conduction of such interfaces. van der Waals cross interfaces are commonly found in low-dimensional structures. Therefore, the weak coupling is an important research topic in the thermal conduction of low-dimensional structures. In folded 2D materials, such as folded graphene, the presence of a large number of van der Waals cross interfaces makes weak phonon coupling an important factor because of its thermal conductivity, as demonstrated in simulation studies of folded graphene sheets [184,185]. By contrast, in double-wall nanotubes, the van der Waals force among nanotubes of different diameters leads to weak phonon coupling. In the study of double-wall nanotubes, the strength of the interactions among the tubes remarkably affects the phonon transport, and when the strength of the interactions was set well beyond the van der Waals forces, the weak phonon coupling disappeared, and the thermal conductivity decreased markedly, indicating that weak phonon coupling plays an important role in phonon transport [184,186].

Therefore, weak phonon coupling, as a crucial physical mechanism, demonstrates a prominent role in fundamental research and industrial applications such as electronics and thermoelectrics [16]. The in-depth study of weak phonon coupling could provide a comprehensive understanding and exploration of low-dimensional nanostructures. However, at present, related studies focus more on experiments and simulations, lacking generally accepted analytical results or theories. Meanwhile, the current weak phonon coupling [39] model is based on the Boltzmann transport equation, which is only applicable to the case of particle transport. As the characteristic size of systems becomes smaller, the wave-like properties of the phonon transport within the nanostructure are improved [80]. Therefore, the wave-like properties must be incorporated to obtain a more accurate description, which needs further investigation.

5 High-order anharmonicity

The lattice thermal conductivity of solids is determined on the basis of a combination of various phonon scattering processes, including point defect, isotope, surface, and phonon-phonon anharmonic scattering [187-189]. Three-phonon scattering is regarded as the lowest order anharmonic interaction, and four-phonon scattering is a high-order anharmonic interaction. As shown in Figure 5, in three-phonon scattering processes, two phonons can combine to generate a

new phonon, or one phonon can split into two phonons. In four-phonon scattering, three possible processes are identified, that is, one phonon splits into three phonons; three phonons combine to generate a new phonon, or two phonons interact and create two new phonons.

The study of four-phonon scattering has a long history [190-192]. In experiments, the importance of a four-phonon process can be determined on the basis of temperature-dependent thermal conductivity. The Debye theory suggests that at sufficiently high temperature, the lattice thermal conductivity limited by three-phonon scattering should decrease with the increase of temperature to $1/T$. However, if the four-phonon scattering rate is strong, then it should be corrected as follows [190]:

$$\frac{1}{\kappa} = aT + bT^2, \tag{3}$$

where the linear term is dominated by three-phonon processes, and the quadratic term is ascribed to four-phonon processes. The phonon scattering rate for four-phonon processes was first discussed by Pomeranchuk [191] in 1941 with a potential function for solids, including the quartic term in atomic displacements. Ecsedy and Klemens [192] developed a theorem to calculate the three-phonon and four-phonon scattering rates based on terms of Grüneisen coefficients. Based on their theorem, the four-phonon scattering rate depends on the square of the phonon frequency and the square of the temperature. In addition, four-phonon scattering is weaker than the three-phonon processes even at high temperature. A rigorous estimation indicated that in most solids, the ratio of the four-phonon scattering rate to the three-phonon scattering rate is less than 10^{-2} even at 1000 K. Recently, Feng and Ruan [193] developed formalism to determine the scattering probability explicitly for four-phonon scattering. This formalism has also been applied to study the effect of quartic anharmonicity on the thermal conductivity of a complex crystal [194], binary rocksalt, and zinc blende compounds [195]. A more detailed discussion about four-phonon scattering formalism can be found in a recent review [196].

Lindsay and Broido [197] calculated the thermal conductivity and phonon scattering phase space of different semiconductors. In some semiconductors, the phase space for four-phonon scattering may be larger than three-phonon scattering. For example, in InP, the four-phonon phase space is 13 times larger than three-phonon processes because three-phonon scattering involves two acoustic phonon modes, and one optical phonon mode is nearly frozen out. However, despite the high phase space, the room temperature scattering rates for four-phonon coupling are a hundred times weaker than the scattering rates of three-phonon processes. Therefore, in InP, four-phonon scattering still has little contribution to the lattice thermal conductivity at room temperature and below.

In four-phonon scattering, the complexity of the theory increases as the number of phonons increases. Moreover, such calculations involve considerable numerical complexity with high computational costs. Considering the slight effect of four-phonon scattering on the total thermal conductivity of most solids, four-phonon scattering is always ignored in calculation by solving the Boltzmann transport equation, and three-phonon scattering may govern thermal conductivity in solids.

In 2017, a significant four-phonon scattering rate was demonstrated in zinc blende BAs [198]. Feng et al. [198] calculated the transition probability of each phonon scattering process based on Fermi's golden rule, and then the three- and four-phonon scattering rates were determined by summing up the probabilities of all possible scattering events. For some phonon modes, the four-phonon scattering strength is comparable to or even stronger than the three-phonon counterparts. The origin of such an unusual phenomenon in BAs is illustrated in Figure 6(a). In BAs bulk, a large acoustic-optical phonon gap is observed; therefore, three-phonon scattering is suppressed because the summation of

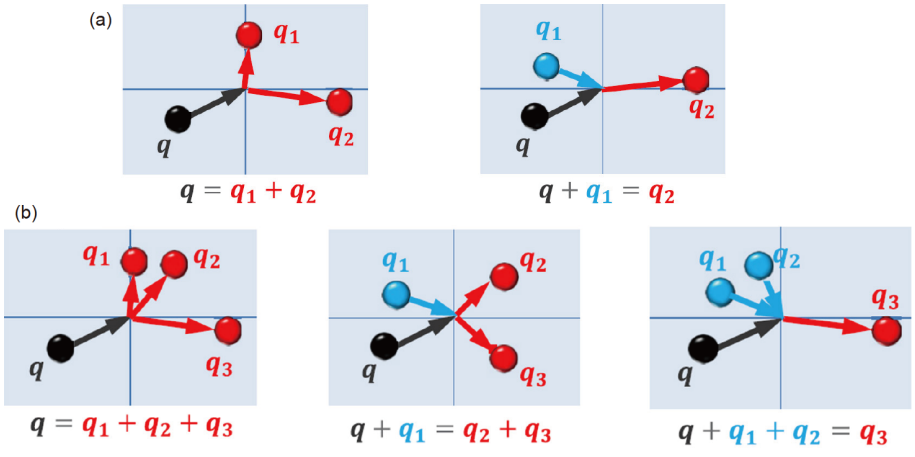

Figure 5 (Color online) (a) Three- and (b) four-phonon scattering diagrams. Here $\boldsymbol{q}$ is the phonon wave vector [199].

the energies of two acoustic phonons is always less than that of one optical phonon. However, it does not hinder four-phonon processes. Therefore, if four-phonon coupling is considered, then the optical phonon relaxation time will reduce remarkably. Compared with three-phonon processes, four-phonon coupling is more crucial at higher temperatures, as more high-frequency phonons are excited with temperature. Therefore, the thermal conductivity of BAs is remarkably reduced if four-phonon scattering is included (Figure 6(b)). At room temperature, the calculated value of thermal conductivity is reduced from 2200 to 1400 W/(m K) with four-phonon anharmonicity. On the contrary, in materials without large acoustic-optical phonon gaps, such as Si and diamond, energy conservation and momentum conservation can be simultaneously achieved for three-phonon scattering; thus, four-phonon scattering is not so important.

In monolayer graphene, although phonon scattering involving three out-of-plane (ZA) phonons is forbidden because of the symmetry selection rule, the four-ZA-phonon scattering is allowed. Given the quadratic characteristic in the dispersion of ZA phonons, a large population of low-frequency ZA phonons is observed, resulting in high four-phonon scattering strength. Solving the linearized phonon Boltzmann transport equation by combining the force constants provided from zero-temperature density functional theory calculation, Feng and Ruan [199] re-visited the lattice thermal conductivity of monolayer graphene, including three- and four-phonon scattering. Compared with three-phonon scattering, the relative contribution of the ZA phonon will reduce from 70% to 30% if four-phonon coupling is included. Moreover, most of these four-phonon processes are normal processes. Therefore, for monolayer graphene, considering four-phonon scattering, the phonon hydrodynamic characteristic should be evident [200]. On the contrary, the four-phonon scattering in multilayer graphene and graphite is not remarkable because of the ZA splitting induced by interlayer van der Waals interaction.

Notably, the effects of high-order anharmonicity on the absolute value of thermal conductivity are complex. Here we used PbTe as an example to demonstrate the effects of high-order anharmonicity. We selected PbTe because PbTe-based thermoelectric materials have attracted great research attention in recent years because of their low lattice thermal conductivity [201-203]. In 2018, Xia [204] studied the lattice thermal conductivity of PbTe by considering three-phonon and four-phonon anharmonicity, anharmonic phonon renormalization, and thermal expansion at finite temperature. Given the low Debye temperature in PbTe (136 K), high-order anharmonicity plays an important role in determining the phonon scattering strength. In that work, the temperature-induced anharmonic phonon renormalization (APRN) at finite temperature is included on top of the quasi-harmonic approximation (QHA) calculation. At room temperature, the experimental thermal conductivity of single-crystal PbTe is approximately 2.5-2.6 W/(m K) [205]. Considering three-phonon scattering and APRN on top of QHA calculation, the calculated value of thermal conductivity is approximately 4 W/(m K). However, if four-phonon scattering is included, then the value of thermal conductivity reduces to 2.6 W/(m K) at 300 K, which is consistent with the experimental value. Detailed analysis indicates that APRN and four-phonon scattering play a crucial role in providing an accurate theoretical value of thermal conductivity. If anharmonic phonon renormalization is ignored, then the thermal conductivity is lower than the experimental value because of the underestimation of contribution from acoustic phonons. The underlying mechanism shows that anharmonic phonon renormalization can lead to reduced phonon scattering phase space because of the strong vibrational frequency shift. Therefore, considering the high-order phonon anharmonicity to calculate the thermal conductivity, the anharmonic phonon renormalization must be included to provide appropriate

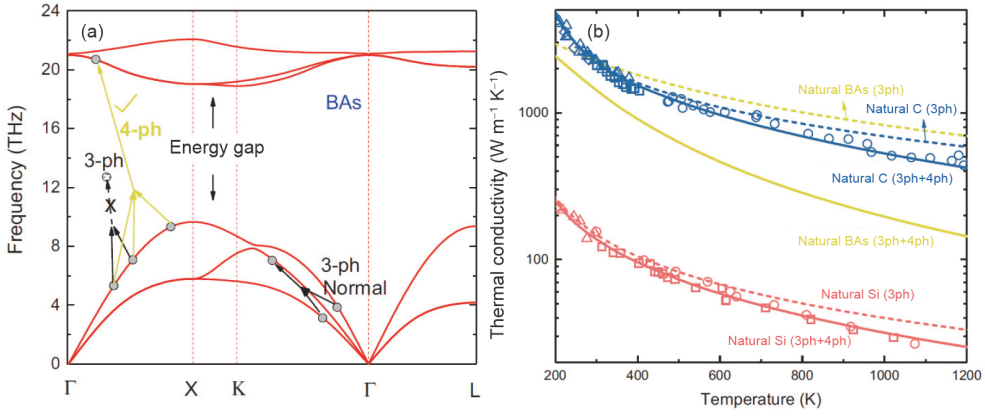

Figure 6 (Color online) (a) Phonon dispersion of BAs and possible three- and four-phonon scattering processes. Considering the large frequency gap between acoustic and optical phonons, three-phonon processes are suppressed with intra-band scattering. On the contrary, the four-phonon process is contributed by inner- and inter-band scattering processes. (b) Thermal conductivities of naturally occurring BAs, Si, and diamond. Here the dashed lines indicate calculated values by considering three-phonon scattering, and solid lines indicate the thermal conductivity, including four-phonon scattering. For more details, please refer to ref. [199].

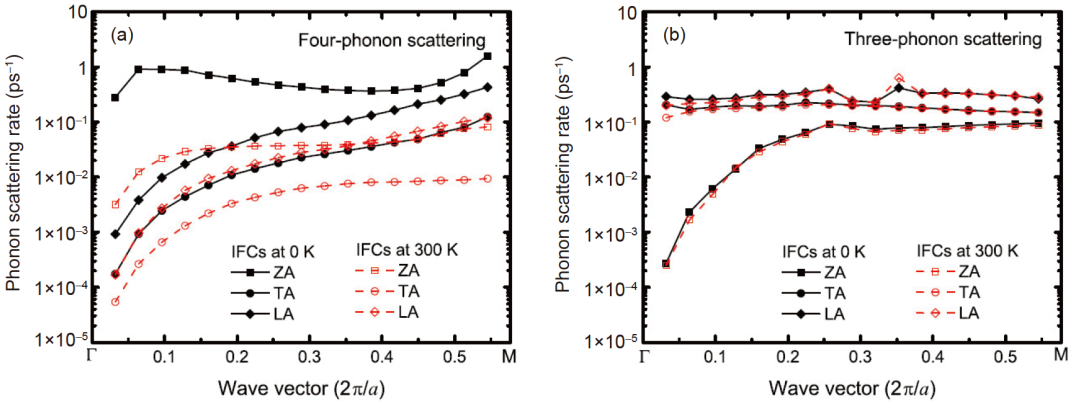

Figure 7 (Color online) (a) Four-phonon and (b) three-phonon scattering rates of graphene with/without using temperature-dependent IFCs [158].

phonon scattering phase space.

Although the effect of four-phonon scattering on thermal conductivity of monolayer graphene has been reported [199], the force constants used in most phonon Boltzmann transport equation calculations were extracted at 0 K. Compared with the phonon dispersion calculated from 0 K force constant, the temperature-dependent force constants would result in different anharmonic characteristic and change in phonon frequency. In calculating the phonon scattering rates, energy conservation conditions before and after scattering must be satisfied. Thus, the phonon frequency shift has a certain effect on the phonon scattering rate and thermal conductivity. Gu et al. [158] studied the effect of temperature-dependent interatomic force constants on the calculated thermal conductivity of monolayer graphene by solving the phonon Boltzmann transport equation. As shown in Figure 7(a), when the force constants at 300 K are used, the four-phonon scattering rates are almost lower by an order of magnitude than those calculated by using the force constants at 0 K. However, the three-phonon scattering rates are less sensitive to the temperature dependence in force constants (Figure 7(b). Therefore, if force constants at 0 K are adopted, then the importance of four-phonon scattering may be overestimated. This work expands the understanding of three-phonon and four-phonon scattering at finite temperature.

6 Conclusion and outlook

In this review, we present a state-of-the-art view of several emerging phononic physics phenomena, which have attracted extensive research attention in recent years. First, phonon coherence and its effects on phonon localization and thermal conductivity are comprehensively discussed. Then, topological phonons and material candidates to observe topological phonons are comprehensively discussed. Next, the weak coupling among phonons in low-dimensional systems has also been addressed. Finally, the high-order phonon anharmonicity and its effect on thermal conductivity are presented. Therefore, the insights summarized in our review can provide important references and guidelines for future studies on thermal conduction in solid materials.

Despite remarkable advancements in theoretical [187] and experimental [206] understanding of the phonon transport, further investigations combining experimental and theoretical efforts remain indispensable because of the complexity of phononic physics. Furthermore, the thermal conductivity of solid materials results from a combination of the above-mentioned mechanisms and principles. In principle, these mechanisms manifest themselves as the major ones in different application scopes and characteristics, and exploring the effect of multi-mechanism on the phonon transport in the same material remains a difficult task. Therefore, we hypothesize that phonon thermal conduction in solid materials remains an active research topic, and the continuous experimental and theoretical studies can boost further advancement in a wide variety of applications.

Jie Chen was supported in part by the National Natural Science Foundation of China (Grant Nos. 11890703, and 12075168), the Science and Technology Commission of Shanghai Municipality (Grant Nos. 19ZR1478600, and 21JC1405600), and the Fundamental Research Funds for the Central Universities (Grant No. 22120220060). Gang Zhang was supported in part by the RIE2020 Advanced Manufacturing and Engineering (AME) Programmatic (Grant No. A1898b0043), and Singapore Aerospace Programme Cycle 15 (Grant No. M2115a0092). Jiaojiao Zhu and Shengyuan A. Yang are supported by the Singapore Ministry of Education AcRF Tier 2 (Grant No. T2EP50220-0026).

1 J. Chen, X. Xu, J. Zhou, and B. Li, Rev. Mod. Phys. **94**, 025002 (2022).
2 Y. Fu, J. Hansson, Y. Liu, S. Chen, A. Zehri, M. K. Samani, N. Wang, Y. Ni, Y. Zhang, Z. B. Zhang, Q. Wang, M. Li, H. Lu, M. Sledzinska, C. M. S. Torres, S. Volz, A. A. Balandin, X. Xu, and J. Liu, 2D Mater. **7**, 012001 (2020).
3 Y. Ouyang, Z. Zhang, D. Li, J. Chen, and G. Zhang, Annalen Der Physik **531**, 1800437 (2019).
4 J. He, Y. Hu, D. Li, and J. Chen, Nano Res. **15**, 3804 (2022).
5 G. Chen, Nat. Rev. Phys. **3**, 555 (2021).

6 Z. Zhang, Y. Ouyang, Y. Cheng, J. Chen, N. Li, and G. Zhang, Phys. Rep. **860**, 1 (2020).
7 X. Gu, Y. Wei, X. Yin, B. Li, and R. Yang, Rev. Mod. Phys. **90**, 041002 (2018), arXiv: 1705.06156.
8 X. Xu, J. Chen, and B. Li, J. Phys.-Condens. Matter **28**, 483001 (2016).
9 N. Yang, G. Zhang, and B. Li, Nano Today **5**, 85 (2010).
10 D. G. Cahill, P. V. Braun, G. Chen, D. R. Clarke, S. Fan, K. E. Goodson, P. Keblinski, W. P. King, G. D. Mahan, A. Majumdar, H. J. Maris, S. R. Phillpot, E. Pop, and L. Shi, Appl. Phys. Rev. **1**, 011305 (2014).
11 W. Ren, Y. Ouyang, P. Jiang, C. Yu, J. He, and J. Chen, Nano Lett. **21**, 2634 (2021).
12 J. H. Seol, I. Jo, A. L. Moore, L. Lindsay, Z. H. Aitken, M. T. Pettes, X. Li, Z. Yao, R. Huang, D. Broido, N. Mingo, R. S. Ruoff, and L. Shi, Science **328**, 213 (2010).
13 L. Lindsay, D. A. Broido, and T. L. Reinecke, Phys. Rev. Lett. **109**, 095901 (2012).
14 W. Li, J. Carrete, N. A. Katcho, and N. Mingo, Comput. Phys. Commun. **185**, 1747 (2014).
15 J. S. Wang, J. Wang, and J. T. Lü, Eur. Phys. J. B **62**, 381 (2008), arXiv: 0802.2761.
16 H. Song, J. Liu, B. Liu, J. Wu, H. M. Cheng, and F. Kang, Joule **2**, 442 (2018).
17 S. Lu, Y. Ouyang, C. Yu, P. Jiang, J. He, and J. Chen, J. Appl. Phys. **129**, 225106 (2021).
18 G. Fugallo, A. Cepellotti, L. Paulatto, M. Lazzeri, N. Marzari, and F. Mauri, Nano Lett. **14**, 6109 (2014).
19 Z. Wang, J. E. Alaniz, W. Jang, J. E. Garay, and C. Dames, Nano Lett. **11**, 2206 (2011).
20 Y. Ouyang, Z. Zhang, C. Yu, J. He, G. Yan, and J. Chen, Chin. Phys. Lett. **37**, 126301 (2020).
21 K. T. Regner, D. P. Sellan, Z. Su, C. H. Amon, A. J. H. McGaughey, and J. A. Malen, Nat. Commun. **4**, 1640 (2013).
22 B. Poudel, Q. Hao, Y. Ma, Y. Lan, A. Minnich, B. Yu, X. Yan, D. Wang, A. Muto, D. Vashaee, X. Chen, J. Liu, M. S. Dresselhaus, G. Chen, and Z. Ren, Science **320**, 634 (2008).
23 M. N. Luckyanova, J. Garg, K. Esfarjani, A. Jandl, M. T. Bulsara, A. J. Schmidt, A. J. Minnich, S. Chen, M. S. Dresselhaus, Z. Ren, E. A. Fitzgerald, and G. Chen, Science **338**, 936 (2012).
24 S. Lee, K. Hippalgaonkar, F. Yang, J. Hong, C. Ko, J. Suh, K. Liu, K. Wang, J. J. Urban, X. Zhang, C. Dames, S. A. Hartnoll, O. Delaire, and J. Wu, Science **355**, 371 (2012).
25 X. Xu, J. Zhou, and J. Chen, Adv. Funct. Mater. **30**, 1904704 (2020).
26 R. Hu, S. Iwamoto, L. Feng, S. Ju, S. Hu, M. Ohnishi, N. Nagai, K. Hirakawa, and J. Shiomi, Phys. Rev. X **10**, 021050 (2020).
27 J. Dai, and Z. Tian, Phys. Rev. B **101**, 041301 (2020), arXiv: 1910.01266.
28 Z. Chen, and C. Dames, Appl. Phys. Lett. **107**, 193104 (2015).
29 A. Giri, and P. E. Hopkins, Adv. Funct. Mater. **30**, 1903857 (2020).
30 Y. Ouyang, C. Yu, G. Yan, and J. Chen, Front. Phys. **16**, 43200 (2021).
31 S. Lee, D. Broido, K. Esfarjani, and G. Chen, Nat. Commun. **6**, 6290 (2015).
32 A. Cepellotti, G. Fugallo, L. Paulatto, M. Lazzeri, F. Mauri, and N. Marzari, Nat. Commun. **6**, 6400 (2015).
33 C. Yu, Y. Ouyang, and J. Chen, J. Appl. Phys. **130**, 010902 (2021).
34 G. Xie, D. Ding, and G. Zhang, Adv. Phys. X **3**, 1480417 (2018), arXiv: 1806.03401.
35 R. Anufriev, J. Maire, and M. Nomura, APL Mater. **9**, 070701 (2021).
36 Z. Zhang, Y. Guo, M. Bescond, J. Chen, M. Nomura, and S. Volz, APL Mater. **9**, 081102 (2021).
37 V. Z. Kresin, and S. A. Wolf, Rev. Mod. Phys. **81**, 481 (2009), arXiv: 0904.2038.
38 Z. Zhang, Y. Guo, M. Bescond, J. Chen, M. Nomura, and S. Volz, Phys. Rev. Lett. **128**, 015901 (2022), arXiv: 2110.09750.
39 C. Deng, Y. Huang, M. An, and N. Yang, Mater. Today Phys. **16**, 100305 (2021).
40 F. Tian, B. Song, X. Chen, N. K. Ravichandran, Y. Lv, K. Chen, S. Sullivan, J. Kim, Y. Zhou, T. H. Liu, M. Goni, Z. Ding, J. Sun, G. A. G. Udalamatta Gamage, H. Sun, H. Ziyaee, S. Huyan, L. Deng, J. Zhou, A. J. Schmidt, S. Chen, C. W. Chu, P. Y. Huang, D. Broido, L. Shi, G. Chen, and Z. Ren, Science **361**, 582 (2018).
41 J. S. Kang, M. Li, H. Wu, H. Nguyen, and Y. Hu, Science **361**, 575 (2018).
42 S. Li, Q. Zheng, Y. Lv, X. Liu, X. Wang, P. Y. Huang, D. G. Cahill, and B. Lv, Science **361**, 579 (2018).
43 T. T. Zhang, H. Miao, Q. Wang, J. Q. Lin, Y. Cao, G. Fabbris, A. H. Said, X. Liu, H. C. Lei, Z. Fang, H. M. Weng, and M. P. M. Dean, Phys. Rev. Lett. **123**, 245302 (2019), arXiv: 1910.13637.
44 T. Zhang, Z. Song, A. Alexandradinata, H. Weng, C. Fang, L. Lu, and Z. Fang, Phys. Rev. Lett. **120**, 016401 (2018), arXiv: 1705.07244.
45 L. Zhang, J. Ren, J. S. Wang, and B. Li, Phys. Rev. Lett. **105**, 225901 (2010), arXiv: 1008.0458.
46 D. A. Broido, M. Malorny, G. Birner, N. Mingo, and D. A. Stewart, Appl. Phys. Lett. **91**, 231922 (2007).
47 O. Hellman, and D. A. Broido, Phys. Rev. B **90**, 134309 (2014).
48 D. A. Broido, L. Lindsay, and A. Ward, Phys. Rev. B **86**, 115203 (2012).
49 W. Li, N. Mingo, L. Lindsay, D. A. Broido, D. A. Stewart, and N. A. Katcho, Phys. Rev. B **85**, 195436 (2012).
50 S. Lu, W. Ren, J. He, C. Yu, P. Jiang, and J. Chen, Phys. Rev. B **105**, 165301 (2022).
51 J. Maire, R. Anufriev, R. Yanagisawa, A. Ramiere, S. Volz, and M. Nomura, Sci. Adv. **3**, e1700027 (2017), arXiv: 1508.04574.
52 J. Ravichandran, A. K. Yadav, R. Cheaito, P. B. Rossen, A. Soukiassian, S. J. Suresha, J. C. Duda, B. M. Foley, C. H. Lee, Y. Zhu, A. W. Lichtenberger, J. E. Moore, D. A. Muller, D. G. Schlom, P. E. Hopkins, A. Majumdar, R. Ramesh, and M. A. Zurbuchen, Nat. Mater. **13**, 168 (2013).
53 M. Maldovan, Nat. Mater. **14**, 667 (2015).
54 J. Lee, W. Lee, G. Wehmeyer, S. Dhuey, D. L. Olynick, S. Cabrini, C. Dames, J. J. Urban, and P. Yang, Nat. Commun. **8**, 14054 (2017).
55 N. Yang, G. Zhang, and B. Li, Nano Lett. **8**, 276 (2008), arXiv: 0712.0949.
56 Z. Wang, and N. Mingo, Appl. Phys. Lett. **97**, 101903 (2010), arXiv: 1104.1570.
57 L. Shi, D. Yao, G. Zhang, and B. Li, Appl. Phys. Lett. **96**, 173108 (2010).
58 I. Marginean, J. S. Page, R. T. Kelly, K. Tang, and R. D. Smith, Appl. Phys. Lett. **95**, 184103 (2009).
59 L. Shi, J. Chen, G. Zhang, and B. Li, Phys. Lett. A **376**, 978 (2012).
60 Z. Zhang, J. Chen, and B. Li, Nanoscale **9**, 14208 (2017).
61 M. V. Simkin, and G. D. Mahan, Phys. Rev. Lett. **84**, 927 (2000), arXiv: cond-mat/9907368.
62 J. K. Yu, S. Mitrovic, D. Tham, J. Varghese, and J. R. Heath, Nat. Nanotech. **5**, 718 (2010).
63 S. Hu, S. Ju, C. Shao, J. Guo, B. Xu, M. Ohnishi, and J. Shiomi, Mater. Today Phys. **16**, 100324 (2021).
64 S. Hu, Z. Zhang, P. Jiang, W. Ren, C. Yu, J. Shiomi, and J. Chen, Nanoscale **11**, 11839 (2019).
65 J. Oh, H. Yoo, J. Choi, J. Y. Kim, D. S. Lee, M. J. Kim, J. C. Lee, W. N. Kim, J. C. Grossman, J. H. Park, S. S. Lee, H. Kim, and J. G. Son, Nano Energy **35**, 26 (2017).
66 S. Alaie, D. F. Goettler, M. Su, Z. C. Leseman, C. M. Reinke, and I. El-Kady, Nat. Commun. **6**, 7228 (2015).
67 R. Anufriev, J. Maire, and M. Nomura, Phys. Rev. B **93**, 045411 (2016).
68 X. K. Chen, Z. X. Xie, W. X. Zhou, L. M. Tang, and K. Q. Chen, Appl. Phys. Lett. **109**, 023101 (2016).
69 C. da Silva, F. Saiz, D. A. Romero, and C. H. Amon, Phys. Rev. B **93**, 125427 (2016).
70 K. Shinokita, K. Reimann, M. Woerner, T. Elsaesser, R. Hey, and C.

Flytzanis, Phys. Rev. Lett. **116**, 075504 (2016).
71 H. Chen, H. Wang, Y. Yang, N. Li, and L. Zhang, Phys. Rev. E **98**, 032131 (2018).
72 B. Qiu, G. Chen, and Z. Tian, Nanoscale Microscale ThermoPhys. Eng. **19**, 272 (2015).
73 L. Lu, D. Ma, M. Zhong, and L. Zhang, New J. Phys. **24**, 013007 (2022).
74 Z. Zhang, S. Hu, T. Nakayama, J. Chen, and B. Li, Carbon **139**, 289 (2018).
75 B. L. Davis, and M. I. Hussein, Phys. Rev. Lett. **112**, 055505 (2014), arXiv: 1304.6070.
76 D. Ma, X. Wan, and N. Yang, Phys. Rev. B **98**, 245420 (2018), arXiv: 1810.04841.
77 H. Honarvar, and M. I. Hussein, Phys. Rev. B **93**, 081412 (2016), arXiv: 1511.08898.
78 S. Xiong, K. Sääskilahti, Y. A. Kosevich, H. Han, D. Donadio, and S. Volz, Phys. Rev. Lett. **117**, 025503 (2016).
79 H. Honarvar, and M. I. Hussein, Phys. Rev. B **97**, 195413 (2018), arXiv: 1606.08591.
80 D. Ma, A. Arora, S. Deng, G. Xie, J. Shiomi, and N. Yang, Mater. Today Phys. **8**, 56 (2019).
81 P. W. Anderson, Phys. Rev. **109**, 1492 (1958).
82 A. I. Hochbaum, R. Chen, R. D. Delgado, W. Liang, E. C. Garnett, M. Najarian, A. Majumdar, and P. Yang, Nature **451**, 163 (2008).
83 P. Martin, Z. Aksamija, E. Pop, and U. Ravaioli, Phys. Rev. Lett. **102**, 125503 (2009), arXiv: 0902.4735.
84 J. Mendoza, and G. Chen, Nano Lett. **16**, 7616 (2016).
85 M. N. Luckyanova, J. Mendoza, H. Lu, B. Song, S. Huang, J. Zhou, M. Li, Y. Dong, H. Zhou, J. Garlow, L. Wu, B. J. Kirby, A. J. Grutter, A. A. Puretzky, Y. Zhu, M. S. Dresselhaus, A. Gossard, and G. Chen, Sci. Adv. **4**, eaat9460 (2018).
86 R. Hu, and Z. Tian, Phys. Rev. B **103**, 045304 (2021).
87 S. Hu, Z. Zhang, P. Jiang, J. Chen, S. Volz, M. Nomura, and B. Li, J. Phys. Chem. Lett. **9**, 3959 (2018).
88 T. Juntunen, O. Vänskä, and I. Tittonen, Phys. Rev. Lett. **122**, 105901 (2019).
89 Y. Guo, M. Bescond, Z. Zhang, S. Xiong, K. Hirakawa, M. Nomura, and S. Volz, APL Mater. **9**, 091104 (2021), arXiv: 2105.01832.
90 Z. Tian, ACS Nano **13**, 3750 (2019).
91 Y. Wang, H. Huang, and X. Ruan, Phys. Rev. B **90**, 165406 (2014).
92 B. Latour, S. Volz, and Y. Chalopin, Phys. Rev. B **90**, 014307 (2014).
93 P. Jiang, Y. Ouyang, W. Ren, C. Yu, J. He, and J. Chen, APL Mater. **9**, 040703 (2021).
94 S. Hu, L. Feng, C. Shao, I. A. Strelnikov, Y. A. Kosevich, and J. Shiomi, Phys. Rev. B **102**, 024301 (2020), arXiv: 2001.10321.
95 Z. Zhang, S. Hu, Q. Xi, T. Nakayama, S. Volz, J. Chen, and B. Li, Phys. Rev. B **101**, 081402 (2020).
96 Z. Zhang, Y. Ouyang, J. Chen, and S. Volz, Chin. Phys. B **29**, 124402 (2020).
97 S. Rieger, T. Fürmann, J. K. Stolarczyk, and J. Feldmann, Nano Lett. **21**, 7887 (2021).
98 I. Takagi, Y. Kayanuma, and K. G. Nakamura, Phys. Rev. B **104**, 134301 (2021).
99 H. Han, B. Li, S. Volz, and Y. A. Kosevich, Phys. Rev. Lett. **114**, 145501 (2015).
100 M. Simoncelli, N. Marzari, and F. Mauri, Nat. Phys. **15**, 809 (2019), arXiv: 1901.01964.
101 L. Isaeva, G. Barbalinardo, D. Donadio, and S. Baroni, Nat. Commun. **10**, 3853 (2019), arXiv: 1904.02255.
102 A. Jain, Phys. Rev. B **102**, 201201 (2020).
103 Z. Zhang, Y. Guo, M. Bescond, J. Chen, M. Nomura, and S. Volz, Phys. Rev. B **103**, 184307 (2021), arXiv: 2003.02384.
104 Z. Zhang, Y. Guo, M. Bescond, J. Chen, M. Nomura, and S. Volz, npj Comput. Mater. **8**, 96 (2022).
105 Z. Zhang, Y. Guo, M. Bescond, J. Chen, M. Nomura, and S. Volz, J. Appl. Phys. **130**, 084301 (2021).
106 G. S. MacCabe, H. Ren, J. Luo, J. D. Cohen, H. Zhou, A. Sipahigil, M. Mirhosseini, and O. Painter, Science **370**, 840 (2020), arXiv: 1901.04129.
107 G. Heinrich, M. Ludwig, J. Qian, B. Kubala, and F. Marquardt, Phys. Rev. Lett. **107**, 043603 (2011), arXiv: 1007.4819.
108 D. J. Thouless, M. Kohmoto, M. P. Nightingale, and M. den Nijs, Phys. Rev. Lett. **49**, 405 (1982).
109 C. K. Chiu, J. C. Y. Teo, A. P. Schnyder, and S. Ryu, Rev. Mod. Phys. **88**, 035005 (2016), arXiv: 1505.03535.
110 M. Z. Hasan, and C. L. Kane, Rev. Mod. Phys. **82**, 3045 (2010), arXiv: 1002.3895.
111 X. L. Qi, and S. C. Zhang, Rev. Mod. Phys. **83**, 1057 (2011), arXiv: 1008.2026.
112 C. Strohm, G. L. J. A. Rikken, and P. Wyder, Phys. Rev. Lett. **95**, 155901 (2005).
113 T. Qin, J. Zhou, and J. Shi, Phys. Rev. B **86**, 104305 (2012), arXiv: 1111.1322.
114 L. Zhang, and Q. Niu, Phys. Rev. Lett. **115**, 115502 (2015).
115 H. Chen, W. Wu, S. A. Yang, X. Li, and L. Zhang, Phys. Rev. B **100**, 094303 (2019).
116 H. Chen, W. Zhang, Q. Niu, and L. Zhang, 2D Mater. **6**, 012002 (2019).
117 M. Gao, W. Zhang, and L. Zhang, Nano Lett. **18**, 4424 (2018).
118 X. Xu, H. Chen, and L. Zhang, Phys. Rev. B **98**, 134304 (2018).
119 X. Chen, X. Lu, S. Dubey, Q. Yao, S. Liu, X. Wang, Q. Xiong, L. Zhang, and A. Srivastava, Nat. Phys. **15**, 221 (2018).
120 Z. Li, T. Wang, C. Jin, Z. Lu, Z. Lian, Y. Meng, M. Blei, M. Gao, T. Taniguchi, K. Watanabe, T. Ren, T. Cao, S. Tongay, D. Smirnov, L. Zhang, and S. F. Shi, ACS Nano **13**, 14107 (2019).
121 Z. Li, T. Wang, C. Jin, Z. Lu, Z. Lian, Y. Meng, M. Blei, S. Gao, T. Taniguchi, K. Watanabe, T. Ren, S. Tongay, L. Yang, D. Smirnov, T. Cao, and S. F. Shi, Nat. Commun. **10**, 2469 (2019), arXiv: 1905.03893.
122 H. Zhu, J. Yi, M. Y. Li, J. Xiao, L. Zhang, C. W. Yang, R. A. Kaindl, L. J. Li, Y. Wang, and X. Zhang, Science **359**, 579 (2018).
123 X. Li, C. Xia, Y. Pan, M. Gao, H. Chen, and L. Zhang, Phys. Rev. B **104**, 054103 (2021).
124 H. Chen, W. Wu, J. Zhu, S. A. Yang, and L. Zhang, Nano Lett. **21**, 3060 (2021).
125 H. Chen, W. Wu, J. Zhu, Z. Yang, W. Gong, W. Gao, S. A. Yang, and L. Zhang, Nano Lett. **22**, 1688 (2022), arXiv: 2109.08872.
126 C. L. Kane, and T. C. Lubensky, Nat. Phys. **10**, 39 (2014), arXiv: 1308.0554.
127 Z. Yang, F. Gao, X. Shi, X. Lin, Z. Gao, Y. Chong, and B. Zhang, Phys. Rev. Lett. **114**, 114301 (2015), arXiv: 1411.7100.
128 S. D. Huber, Nat. Phys. **12**, 621 (2016).
129 Y. Liu, C. S. Lian, Y. Li, Y. Xu, and W. Duan, Phys. Rev. Lett. **119**, 255901 (2017), arXiv: 1708.06482.
130 Y. Liu, Y. Xu, S. C. Zhang, and W. Duan, Phys. Rev. B **96**, 064106 (2017), arXiv: 1606.08013.
131 J. Zhu, W. Wu, J. Zhao, C. Chen, Q. Wang, X. L. Sheng, L. Zhang, Y. X. Zhao, and S. A. Yang, Phys. Rev. B **105**, 085123 (2022), arXiv: 2110.10420.
132 R. Wang, B. W. Xia, Z. J. Chen, B. B. Zheng, Y. J. Zhao, and H. Xu, Phys. Rev. Lett. **124**, 105303 (2020), arXiv: 1908.09447.
133 Q. B. Liu, Z. Wang, and H. H. Fu, Phys. Rev. B **103**, L161303 (2021).
134 C. Xie, Y. Liu, Z. Zhang, F. Zhou, T. Yang, M. Kuang, X. Wang, and G. Zhang, Phys. Rev. B **104**, 045148 (2021).
135 Z. J. Chen, R. Wang, B. W. Xia, B. B. Zheng, Y. J. Jin, Y. J. Zhao, and H. Xu, Phys. Rev. Lett. **126**, 185301 (2021), arXiv: 2103.00920.
136 Z. M. Yu, W. Wu, X. L. Sheng, Y. X. Zhao, and S. A. Yang, Phys. Rev. B **99**, 121106 (2019), arXiv: 1807.02659.
137 Z. Zhang, Z. M. Yu, and S. A. Yang, Phys. Rev. B **103**, 115112 (2021), arXiv: 2101.12477.
138 S. Li, Z. M. Yu, Y. Liu, S. Guan, S. S. Wang, X. Zhang, Y. Yao, and S. A. Yang, Phys. Rev. B **96**, 081106 (2017). ; X. Zhang, Z. M. Yu, Y. Lu, X. L. Sheng, H. Y. Yang, and S. A. Yang, Phys. Rev. B **97**,

125143 (2018), arXiv: 1802.00905.
139 G. Liu, L. Jin, X. Dai, G. Chen, and X. Zhang, Phys. Rev. B **98**, 075157 (2018), arXiv: 1812.10627.
140 F. Zhou, Z. Zhang, H. Chen, M. Kuang, T. Yang, and X. Wang, Phys. Rev. B **104**, 174108 (2021).
141 B. Zheng, B. Xia, R. Wang, Z. Chen, J. Zhao, Y. Zhao, and H. Xu, Phys. Rev. B **101**, 100303 (2020).
142 B. Zheng, F. Zhan, X. Wu, R. Wang, and J. Fan, Phys. Rev. B **104**, L060301 (2021), arXiv: 2103.04593.
143 Q. B. Liu, H. H. Fu, and R. Wu, Phys. Rev. B **104**, 045409 (2021).
144 H. Miao, T. T. Zhang, L. Wang, D. Meyers, A. H. Said, Y. L. Wang, Y. G. Shi, H. M. Weng, Z. Fang, and M. P. M. Dean, Phys. Rev. Lett. **121**, 035302 (2018), arXiv: 1804.10676.
145 C. Xie, H. Yuan, Y. Liu, X. Wang, and G. Zhang, Phys. Rev. B **104**, 134303 (2021), arXiv: 2108.13746.
146 Q. B. Liu, Z. Q. Wang, and H. H. Fu, Phys. Rev. B **104**, L041405 (2021).
147 Z. M. Yu, W. Wu, Y. X. Zhao, and S. A. Yang, Phys. Rev. B **100**, 041118 (2019), arXiv: 1903.08877.
148 J. Wang, H. Yuan, Z. M. Yu, Z. Zhang, and X. Wang, Phys. Rev. Mater. **5**, 124203 (2021).
149 X. Wang, F. Zhou, T. Yang, M. Kuang, Z. M. Yu, and G. Zhang, Phys. Rev. B **104**, L041104 (2021), arXiv: 2103.15495.
150 J. Wang, H. Yuan, M. Kuang, T. Yang, Z. M. Yu, Z. Zhang, and X. Wang, Phys. Rev. B **104**, L041107 (2021), arXiv: 2105.12000.
151 J. Li, J. Liu, S. A. Baronett, M. Liu, L. Wang, R. Li, Y. Chen, D. Li, Q. Zhu, and X. Q. Chen, Nat. Commun. **12**, 1204 (2021), arXiv: 2006.00705.
152 A. P. Schnyder, S. Ryu, A. Furusaki, and A. W. W. Ludwig, Phys. Rev. B **78**, 195125 (2008), arXiv: 0803.2786.
153 A. Kitaev, AIP Conf. Proc. **1134**, 22 (2009).
154 Y. X. Zhao, and Z. D. Wang, Phys. Rev. Lett. **110**, 240404 (2013), arXiv: 1211.7241.
155 Z. M. Yu, Z. Zhang, G. B. Liu, W. Wu, X. P. Li, R. W. Zhang, S. A. Yang, and Y. Yao, Sci. Bull. **67**, 375 (2022), arXiv: 2102.01517.
156 J. Zhu, W. Wu, J. Zhao, H. Chen, L. Zhang, and S. A. Yang, npj Quantum Mater. **7**, 52 (2022).
157 M. An, Q. Song, X. Yu, H. Meng, D. Ma, R. Li, Z. Jin, B. Huang, and N. Yang, Nano Lett. **17**, 5805 (2017), arXiv: 1702.05237.
158 X. Gu, Z. Fan, H. Bao, and C. Y. Zhao, Phys. Rev. B **100**, 064306 (2019), arXiv: 1904.12731.
159 S. Sullivan, A. Vallabhaneni, I. Kholmanov, X. Ruan, J. Murthy, and L. Shi, Nano Lett. **17**, 2049 (2017), arXiv: 1701.03011.
160 A. K. Vallabhaneni, D. Singh, H. Bao, J. Murthy, and X. Ruan, Phys. Rev. B **93**, 125432 (2016).
161 S. Ghosh, W. Bao, D. L. Nika, S. Subrina, E. P. Pokatilov, C. N. Lau, and A. A. Balandin, Nat. Mater. **9**, 555 (2010), arXiv: 1003.5247.
162 L. M. Woods, D. A. R. Dalvit, A. Tkatchenko, P. Rodriguez-Lopez, A. W. Rodriguez, and R. Podgornik, Rev. Mod. Phys. **88**, 045003 (2016), arXiv: 1509.03338.
163 S. Lepri, R. Livi, and A. Politi, Phys. Rev. Lett. **78**, 1896 (1997).
164 T. Prosen, and D. K. Campbell, Phys. Rev. Lett. **84**, 2857 (2000), arXiv: chao-dyn/9908021.
165 A. Lippi, and R. Livi, J. Stat. Phys. **100**, 1147 (2000).
166 S. Lepri, Phys. Rep. **377**, 1 (2003).
167 A. Dhar, Adv. Phys. **57**, 457 (2008), arXiv: 0808.3256.
168 L. Wang, B. Hu, and B. Li, Phys. Rev. E **86**, 040101 (2012).
169 G. Zhang, and B. Li, J. Chem. Phys. **123**, 114714 (2005).
170 M. Wang, X. Shan, and N. Yang, Phys. Lett. A **376**, 3514 (2012).
171 G. Zhang, and B. Li, J. Chem. Phys. **123**, 014705 (2005), arXiv: cond-mat/0403393.
172 S. Liu, X. F. Xu, R. G. Xie, G. Zhang, and B. W. Li, Eur. Phys. J. B **85**, 337 (2012), arXiv: 1205.3065.
173 Z. Lu, A. Vallabhaneni, B. Cao, and X. Ruan, Phys. Rev. B **98**, 134309 (2018).
174 Z. Lu, J. Shi, and X. Ruan, J. Appl. Phys. **125**, 085107 (2019).
175 N. Yang, S. Hu, D. Ma, T. Lu, and B. Li, Sci. Rep. **5**, 14878 (2015), arXiv: 1409.2236.
176 D. Ma, H. Ding, X. Wang, N. Yang, and X. Zhang, Int. J. Heat Mass Transfer **108**, 940 (2017).
177 C. Zhang, D. Ma, M. Shang, X. Wan, J. T. Lü, Z. Guo, B. Li, and N. Yang, Mater. Today Phys. **22**, 100605 (2022).
178 J. Yang, Y. Yang, S. W. Waltermire, X. Wu, H. Zhang, T. Gutu, Y. Jiang, Y. Chen, A. A. Zinn, R. Prasher, T. T. Xu, and D. Li, Nat. Nanotech. **7**, 91 (2011).
179 P. E. Hopkins, ISRN Mech. Eng. **2013**, 1 (2013).
180 R. Xiang, T. Inoue, Y. Zheng, A. Kumamoto, Y. Qian, Y. Sato, M. Liu, D. Tang, D. Gokhale, J. Guo, K. Hisama, S. Yotsumoto, T. Ogamoto, H. Arai, Y. Kobayashi, H. Zhang, B. Hou, A. Anisimov, M. Maruyama, Y. Miyata, S. Okada, S. Chiashi, Y. Li, J. Kong, E. I. Kauppinen, Y. Ikuhara, K. Suenaga, and S. Maruyama, Science **367**, 537 (2020), arXiv: 1807.06154.
181 H. Meng, S. Maruyama, R. Xiang, and N. Yang, Int. J. Heat Mass Transfer **180**, 121773 (2021).
182 W. Feng, X. Yu, Y. Wang, D. Ma, Z. Sun, C. Deng, and N. Yang, Phys. Chem. Chem. Phys. **21**, 25072 (2019), arXiv: 1906.09751.
183 Y. Xiong, X. Yu, Y. Huang, J. Yang, L. Li, N. Yang, and D. Xu, Mater. Today Phys. **11**, 100139 (2019).
184 N. Yang, X. Ni, J. W. Jiang, and B. Li, Appl. Phys. Lett. **100**, 093107 (2012), arXiv: 1207.0285.
185 Q. Song, M. An, X. Chen, Z. Peng, J. Zang, and N. Yang, Nanoscale **8**, 14943 (2016).
186 C. Deng, X. Yu, X. Huang, and N. Yang, J. Heat Transfer **139**, 054504 (2017).
187 G. Zhang, and Y. W. Zhang, Chin. Phys. B **26**, 034401 (2017).
188 C. Yu, Y. Hu, J. He, S. Lu, D. Li, and J. Chen, Appl. Phys. Lett. **120**, 132201 (2022).
189 Y. Ouyang, C. Yu, J. He, P. Jiang, W. Ren, and J. Chen, Phys. Rev. B **105**, 115202 (2022).
190 Y. P. Joshi, M. D. Tiwari, and G. S. Verma, Phys. Rev. B **1**, 642 (1970).
191 I. Pomeranchuk, Phys. Rev. **60**, 820 (1941).
192 D. J. Ecsedy, and P. G. Klemens, Phys. Rev. B **15**, 5957 (1977).
193 T. Feng, and X. Ruan, Phys. Rev. B **93**, 045202 (2016), arXiv: 1510.00706.
194 Y. Xia, K. Pal, J. He, V. Ozoliņš, and C. Wolverton, Phys. Rev. Lett. **124**, 065901 (2020).
195 Y. Xia, V. I. Hegde, K. Pal, X. Hua, D. Gaines, S. Patel, J. He, M. Aykol, and C. Wolverton, Phys. Rev. X **10**, 041029 (2020).
196 T. Feng, and X. Ruan, *Nanoscale Energy Transport*, Chapter 2 (IOP Press, 2020). pp. 1-44.
197 L. Lindsay, and D. A. Broido, J. Phys.-Condens. Matter **20**, 165209 (2008).
198 T. Feng, L. Lindsay, and X. Ruan, Phys. Rev. B **96**, 161201 (2017).
199 T. Feng, and X. Ruan, Phys. Rev. B **97**, 045202 (2018).
200 Y. Hu, D. Li, Y. Yin, S. Li, G. Ding, H. Zhou, and G. Zhang, Nanotechnology **31**, 335711 (2020).
201 Y. Pei, X. Shi, A. LaLonde, H. Wang, L. Chen, and G. J. Snyder, Nature **473**, 66 (2011).
202 J. P. Heremans, V. Jovovic, E. S. Toberer, A. Saramat, K. Kurosaki, A. Charoenphakdee, S. Yamanaka, and G. J. Snyder, Science **321**, 554 (2008).
203 L. D. Zhao, H. J. Wu, S. Q. Hao, C. I. Wu, X. Y. Zhou, K. Biswas, J. Q. He, T. P. Hogan, C. Uher, C. Wolverton, V. P. Dravid, and M. G. Kanatzidis, Energy Environ. Sci. **6**, 3346 (2013).
204 Y. Xia, Appl. Phys. Lett. **113**, 073901 (2018).
205 G. Z. Bagieva, G. M. Murtuzov, G. D. Abdinova, E. A. Allakhverdiev, and D. S. Abdinov, Inorg Mater. **48**, 789 (2012).
206 R. Wu, R. Z. Zhu, S. H. Zhao, G. Zhang, H. Tian, and T. L. Ren, Sci. China Inf. Sci. **64**, 140401 (2021).